Materials Chemistry and Physics 142 (2013) 165–171

Contents lists available at SciVerse ScienceDirect

Materials Chemistry and Physics

journal homepage: www.elsevier.com/locate/matchemphys

Decarburization mechanisms of WC–Co during thermal spraying: Insights from controlled carbon loss and microstructure characterization

Jianhui Yuan, Qing Zhan, Jing Huang, Siyue Ding, Hua Li*

Key Laboratory of Marine Materials and Related Technologies, Ningbo Institute of Materials Technology and Engineering, Chinese Academy of Sciences, Ningbo 315201, China

HIGHLIGHTS

- Morphological feature of W, W_2C, γ phase, etc, in WC–Co coatings is disclosed.
- Locations of the above decarburization-induced phases are revealed.
- Diffusion-controlled carbon loss is the major decarburization regime in APS WC–Co coatings.

GRAPHICAL ABSTRACT

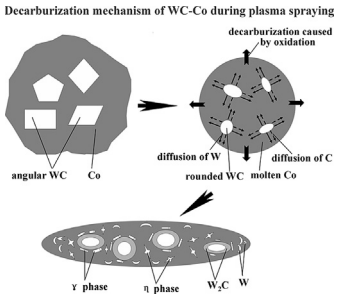

ARTICLE INFO

Article history:
Received 25 February 2013
Received in revised form
20 May 2013
Accepted 25 June 2013

Keywords:
Carbides
Coatings
Electron microscopy
Microstructure
Rietveld analysis

ABSTRACT

Decarburization behavior of WC–Co particles in terms of transformation of WC to W_2C and W, and formation of η and γ phases and microstructure evolution during plasma spraying have been systematically investigated in this study. The extent of the carbon loss of WC was tailored by either altering cooling conditions of substrate/pre-coating or spraying the particles into the media with different temperatures. It is revealed that loss of carbon of WC was alleviated by protection of Co during the coating formation stage. W_2C exhibits epitaxial growth on the WC substrates in perpendicular direction and forms a nearly complete shell around the WC particles. η phase was formed as a result of decarburization and diffusion of associated phases and is located around WC–Co splats with its crystals being in cross shape. The γ phase in rod-like shape with a size of 10–20 nm embeds within the binder Co and is clearly well separated from WC grains. Further decarburization-induced W was detected mainly in Co binder, being apart entirely from WC grains. The main advantage of Co for preventing decarburization in WC–Co particles is not associated with oxidation, but instead the diffusion-controlled carbon loss. These findings would facilitate fabrication of the WC-based cermet coatings with excellent mechanical properties in particular wear resistance for extreme wear applications.

1. Introduction

Thermal sprayed WC-based cermet coatings have been successful in applications against wear encountered by various engineering components. Atmospheric plasma spray (APS), high-velocity oxygen–fuel (HVOF) spray and detonation spray (DS) are the most commonly used techniques for deposition of the coatings.

* Corresponding author. Tel.: +86 574 86686224; fax: +86 574 86685159.
E-mail address: lihua@nimte.ac.cn (H. Li).

0254-0584/$ – see front matter © 2013 Elsevier B.V. All rights reserved.
http://dx.doi.org/10.1016/j.matchemphys.2013.06.052

It is well documented that thermal sprayed WC–Co coatings usually suffer from decomposition and decarburization of the carbide during the spraying [1,2]. The decarburization reduces content of WC in coatings, leading to formation of undesirable phases such as W_2C, W, and amorphous or nanocrystalline Co–W–C phase [3,4]. It has been widely recognized that the overall performance of thermal sprayed WC–Co coatings is significantly affected by the decarburization experienced by the powder particles during spray processing [3–7]. Controlling the decarburization of the carbide is therefore crucial towards achieving the cermet coatings with super mechanical properties. In-depth fundamental understanding of the decarburization behavior during both in-flight and coating formation stages of individual particles is essentially important. Extensive worldwide efforts have been devoted to investigating the decarburization behavior during thermal spraying. It is known that the extent of the decarburization of carbide is closely related to the characteristics of the starting feedstock powders and the heating exerted by the heating source. For example, the decarburization of WC–Co particles was much pronounced when APS was used, in contrast, in the cases of using HVOF or DS process which offers moderate heating for the powders, the extent of the decarburization was substantially lower [2,7,8]. Similarly, spray parameters that play roles in deciding the heating source temperatures [9], e.g. ratio of fuel to oxygen utilized for HVOF or DS, also exhibit remarkable influence on the extent of decarburization of WC–Co depending on the oxidizing nature of the gas [10,11]. In addition, enhanced decarburization of WC–Co has been revealed for the coatings made from WC-based cermet powders with finer WC grains [12,13], most likely due to the overheating of the WC grains during the spraying [10,13,14].

The decarburization mechanisms of WC in WC–Co coatings have been investigated by numerous investigators [11,15–17]. It is reported that the controlling factors for the decarburization in HVOF nano-WC/Co coatings are heterogeneous melting and localized superheating of the high specific surface area of WC in the feeding powders during spraying [15]. A new model for WC–Co decomposition and consequential formation of W, W_2C and an amorphous/nanocrystalline phase in the deposit during spraying was proposed by Stewart et al. [13]. Even though some decarburization theories for thermal sprayed WC–Co coatings were proposed, the knowledge about the decarburization and decarburization-induced microstructural development in WC–Co coatings is not sufficient yet. This study deals with controlling the extent of the decarburization of WC–Co during plasma spraying by altering spray parameters and cooling state of the particles/coatings. The decarburization mechanism was further analyzed by both characterization of the microstructure and chemistry and quantitative detection of the phases in the as-sprayed powders/coatings.

2. Materials and experimental setup

The commercial agglomerated and sintered WC-12wt.% Co powders (H.C. Starck, Germany) with the size range of $-45 + 15$ μm were used in this study. The angular WC grains in the powder particles had a mean size of ~1–5 μm, which were embedded in cobalt binder phase. The original weight percentage of carbon (C) element was 5.38%. For comparison purpose, micron-sized commercial WC powders ($-40 + 20$ μm, Zigong Carbides Co. Ltd., China) were also used as the feedstock. Coating deposition was made by APS-2000K plasma spray system (AVIC Beijing Aeronautical Manufacturing Technology Research Institute, China) on 304L stainless steel plates (10 mm × 20 mm × 2 mm). The spray parameters used in this research were listed in Table 1. The thickness of the as-sprayed coatings was ~300 μm. Prior to the spraying, the substrates were cleaned by sonication in acetone. The WC and WC–Co powders were also sprayed directly into room-temperature distilled water under the same spraying parameters (at a spraying power of 20 kW).

Table 1
Plasma spray parameters.

Primary gas, Ar	42 l min^{-1}
Secondary gas, H_2	11 l min^{-1}
Powder carrier gas, Ar	4 l min^{-1}
Net energy	20 kW
Powder feed rate	46 g min^{-1}
Spray distance	140 mm

X-ray diffraction (XRD, Bruker AXS, Germany) was employed to detect the phases of the samples at a scanning rate of 0.1° s^{-1} using monochromatic Cu-Kα radiation operated at 40 kV. Contents of the phases in the samples were quantified from their XRD spectra using the Rietveld method, a publicly shared software developed by Lutterotti [18]. For the purpose of disclosing the stage at which the decarburization mostly takes place and the extent of the carbon loss at each stage, the as-sprayed WC–Co powders were collected through spraying them into distilled water. The collected powders were dried in a furnace at 50 °C for further analysis. They were analyzed by X-ray photoelectron spectroscope (XPS, AXIS UTL-TRADLD, Shimadzu, Japan) operated at 15 kV and 300 mA. In view of possible contamination of carbon and oxygen on their surfaces, the powders underwent argon etching (Ar^+, 2 kV, 4 μA, 0.3 nm s^{-1}) for 30 s before the XPS detection. The microstructural features of the powders and coatings were characterized using field emission scanning electron microscope (FESEM, FEI Quanta FEG250, the Netherlands). Both the surfaces and the cross-sections of the samples were examined using secondary electron and backscattered electron signals as well. Element analysis was also performed using the energy dispersive system (EDS) equipped with the FESEM. Microhardness of the as-sprayed coatings was assessed by indentation test conducted on their polished cross-sections using a Vickers hardness tester (FLC-50V, Shanghai) under a load of 300 g for 15 s. At least 10 readings were taken for an average value.

3. Results and discussion

In this study, the decarburization of WC at both in-flight stage and coating formation stage of the WC–Co powders was examined separately. For the coating formation stage, the cooling rate is certainly a key factor determining the decarburization extent [15,19]. For thermal sprayed coatings, the splats at different locations in the coatings along through-thickness direction experience

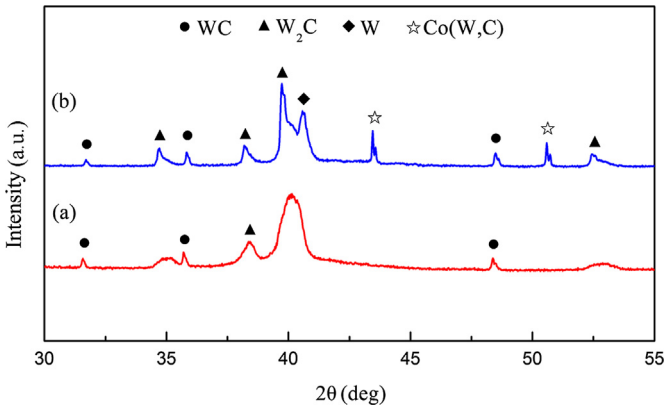

Fig. 1. XRD spectra of the as-sprayed WC–Co coating detected from its bottom side (a) and top side (b).

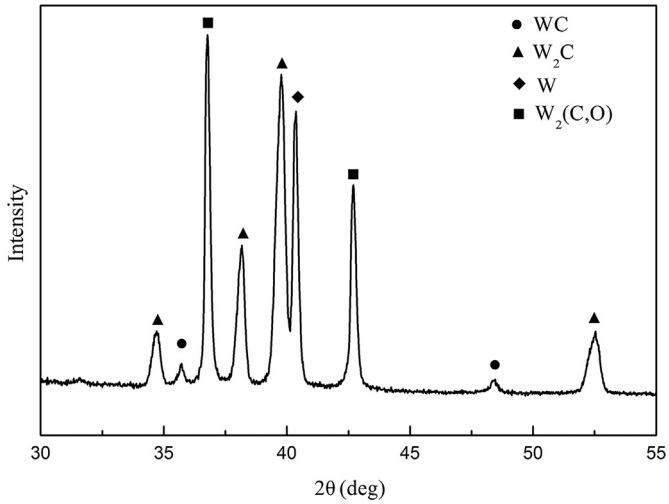

Fig. 2. XRD curve of the plasma-sprayed WC powders collected in room-temperature distilled water.

different cooling rate [20,21]. In this study, the phases at both sides of the WC–Co coatings, top side and bottom side that are in intimate contact with the polished substrate surface, were therefore characterized. XRD detection (Fig. 1a) shows that for the bottom side WC–Co coating, the peaks referring to the phases WC and W_2C are strong, indicating minor decarburization of WC. In addition, there are two broad diffraction peaks, which are located at ~34°–36° and ~39°–41° of 2θ, most likely referring to amorphous or nanocrystalline phases in the coating at its bottom side. The high temperature APS processing favors the reaction between Co and WC, leading to the formation of Co–W–C solid solution phases. In this case, crystalline Co phase was hardly detected in the coating. For the top side coating, however, some sharp diffraction peaks are observed (Fig. 1b), suggesting markedly presence of W_2C, W and Co(W,C). The top side WC–Co coating has a better crystal structure than the bottom side. Appearance of W suggests deteriorated carbon loss of WC at the top side of the coating, which should be directly associated with the relatively lower cooling rate at the top side of the coating. The bottom layer was deposited on room-temperature substrate (no preheating for the polished substrate), while the top layer is composed of the individual splats accumulated on pre-coating with relatively high temperatures due to accumulation of heat flux from the droplets. This phenomenon has been confirmed by Sobolev et al. [22] who observed that the temperature of top side coating was the highest. It was well acknowledged that the process of flattening and solidification of thermal sprayed droplets has completed entirely before impingement of subsequent droplets and each droplet exhibits independent flattening and solidification behavior [23]. The XRD detection results show that the decarburization of WC continued after the impingement of WC–Co droplet on the substrate/pre-coating, extent of which is closely related to its cooling conditions. Further carbon loss of WC to W has been evidenced at the top layer of the coating and this is confirmed to solely happen during the coating formation stage. Previous study has shown that crystalline transition in WC–Co coating occurred at 873 K and Co_6W_6C grew from the coating [24]. It is noted in this study that the Co_6W_6C phase was not detected in the coatings.

The decarburization behavior of the WC–Co powders during the sole in-flight stage was further assessed by analyzing the powders directly sprayed into liquid nitrogen (−196 °C). Due to the extremely low temperature, we speculate here that the phase transformation encountered by WC–Co has been terminated upon its immersion into liquid nitrogen. This in turn offers possibility of acquiring the decarburization data of the WC–Co powders during in-flight stage. It was found that ~71.03% of the WC particles lost their carbon and transformed to W_2C during the in-flight stage, while little amount of W and η phases was detected. To further investigate the effect of binder Co on the decarburization behavior of WC–Co during the spraying, WC particles with the size of −40 + 20 μm were sprayed using the same spray parameters as those employed for WC–Co coating deposition. The as-sprayed WC particles collected in room-temperature distilled water were analyzed and the XRD spectrum is shown in Fig. 2. The prominent peaks for W_2C, W and $W_2(C,O)$ are clear, indicating significant carbon loss of WC. This result is consistent with the observations reported by Khan et al. [25] that WC particles decomposed significantly and almost disappeared after APS. Since the melting point of Co (1495 °C) is much lower than that of WC (2870 °C), Co preferentially melts during APS. Furthermore, the specific heat value of Co (0.42 J g^{-1} K^{-1}) is higher than that of WC (0.05 J g^{-1} K^{-1}), so melting of Co consumes more latent heat [26]. The kinetics of decarburization of WC as described above should be largely dependent on the extent of the heating of the WC particles [27]. It is not surprising

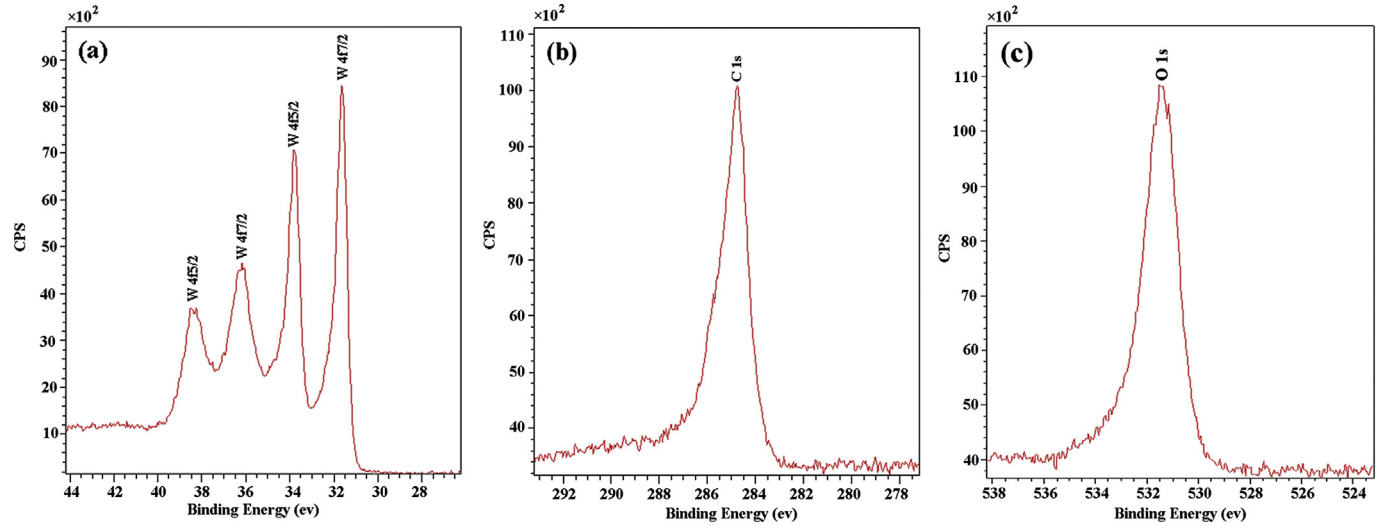

Fig. 3. XPS spectra of the as-sprayed WC–Co powders collected in room-temperature distilled water showing (a) W 4f, (b) C 1s, and (c) O 1s.

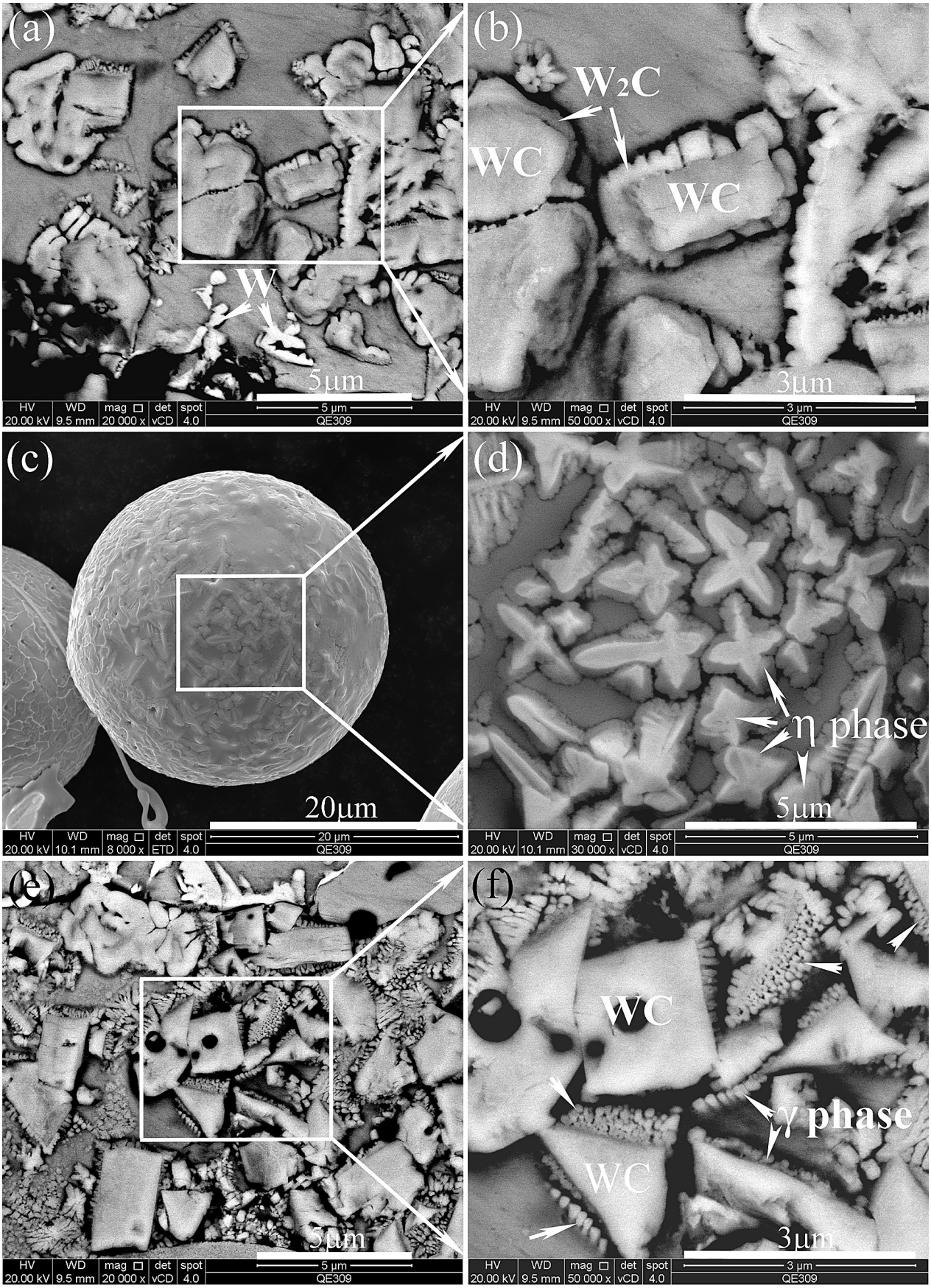
(a)
W
5μm
HV 20.00 kV | WD 9.5 mm | mag 20 000 x | det vCD | spot 4.0 | 5 μm | QE309
(b)
W2C
WC
WC
3μm
HV 20.00 kV | WD 9.5 mm | mag 50 000 x | det vCD | spot 4.0 | 3 μm | QE309
(c)
20μm
HV 20.00 kV | WD 10.1 mm | mag 8 000 x | det ETD | spot 4.0 | 20 μm | QE309
(d)
η phase
5μm
HV 20.00 kV | WD 10.1 mm | mag 30 000 x | det vCD | spot 4.0 | 5 μm | QE309
(e)
5μm
HV 20.00 kV | WD 9.5 mm | mag 20 000 x | det vCD | spot 4.0 | 5 μm | QE309
(f)
WC
γ phase
WC
3μm
HV 20.00 kV | WD 9.5 mm | mag 50 000 x | det vCD | spot 4.0 | 3 μm | QE309

that Co protects WC in the WC–Co powders from intensified heating and consequently alleviates further decarburization.

Changes in valences of W are expected during decarburization of WC–Co particles, it is therefore feasible to estimate the extent of the decarburization by using XPS analysis which can directly detect the valences of W. The XPS spectra of the as-sprayed WC–Co powders collected in distilled water are shown in Fig. 3. According to NIST X-ray Photoelectron Spectroscopy Database [28], coinciding with the detected binding energy peak at 283.3 eV for C, the binding energy peaks of W at 31.5 eV and 33.7 eV are assigned to the phases WC and W_2C respectively. The binding energy peak at 33.4 eV is attributed to alloy W, suggesting severe decarburization of WC to W during the plasma spraying. Furthermore, the binding energy peaks of W at 36.6 and 38.1 eV (which can be deduced to be WO_3 and WO_x [29,30]) and that of O at 531.1 eV (Fig. 3) unambiguously suggest vigorous oxidation of C and W (products of decarburization of WC) during APS.

It has been clear that the decarburization of WC–Co leads to formation of W_2C, W, and Co–W–C, etc, during APS. However, the morphology and distribution of the decarburization products in WC–Co coatings are not clear yet. Microstructure characterization in terms of microstructure evolution might give further insight into decarburization mechanism of WC–Co during APS. BSE image of the as-sprayed WC–Co coatings clearly shows random distribution of the WC particles within the binder phase (Fig. 4). The major element for the bright region shown in Fig. 4a is proven to be W as determined by EDS detection. It is known that in BSE images, the regions with bright and dark color are composed of the elements with higher and lower mean atomic number respectively. It can therefore be concluded that the major component for the bright regions in the WC–Co coating is W. A closer view of the WC–Co coating (Fig. 4b) shows a nearly complete shell around WC particles. The color of the shell is lighter than that of the WC particles. The energy spectrum analysis disclosed the main chemical component of the shell to be ~71 at.%W–29 at.%C, being qualitatively in good agreement with stoichiometry of W_2C. It is very likely that the outer shell around WC particles is W_2C developed directly from the decarburization of WC. The primary carbon loss of WC in terms of formation of W_2C results in formation and growth of the columnar W_2C grains along the direction perpendicular to WC grains. Furthermore, it is clear that the WC particles independently exist in individual splats and were well separated from possible contact with oxygen during the spraying. The decarburization process is usually believed to comprise the following three major reversible reactions [27]:

$$2WC + O_2 \Leftrightarrow W_2C + CO_2 \quad (1)$$

$$2W_2C + O_2 \Leftrightarrow 2W_2(C,O) \quad (2)$$

$$W_2(C,O) \Leftrightarrow 2W + CO \quad (3)$$

However, as revealed in this study, the oxidation might not be the leading reason for the carbon loss of WC to form W_2C. Instead, diffusion of W and C into the binder phase might account mainly for the formation of W_2C. It is well known that WC particles are embedded within the continuous liquid phase during APS. The elements W and C of WC particles diffuse into the liquid phase at high temperatures [2,15]. Due to its higher atomic weight, W diffuses slower than C. Consequently, the concentration of W becomes higher than that of C at the boundary between WC grain and the liquid phase in a short period of time. As soon as the atomic ratio of W/C reaches ~2:1, W_2C is readily formed at this region. At the same time, the interfaces between WC particles and the liquid phase might serve as preferential nucleation sites for W_2C. It is in turn not surprising that W_2C epitaxially grows on the surfaces of WC particles and forms a wrapping structure around WC. Similar morphology and distribution of W_2C in APS WC–Co coatings was also observed by Stewart et al. [13]. In this regard, chemical bond between WC and W_2C grains is possible, while the W_2C grains have irregular shape with a slightly serrated outside border. Further carbon loss already resulted in formation of W, as shown in Fig. 4a (the small white region). Faster dissolution of W into the binder phase is responsible for the "running-away" of W from WC matrix. This study suggests diffusion-controlled carbon loss of WC. Nevertheless, there is still possibility of the oxidation-driven decarburization of WC.

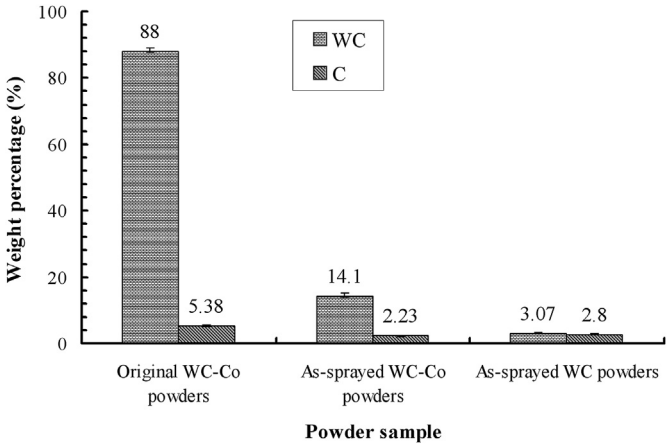

Fig. 5. Weight percentages of WC and C retained in the original WC–Co powders and the as-plasma-sprayed WC–Co and WC powders collected in room-temperature distilled water.

It is well known that Co–W–C solid solution phases such as η or γ phase are brittle in nature and are also detrimental to coating structure due to the decrease in effective metallic binder [31]. Even though formation of η or γ phase is usually unavoidable during coating deposition, few reports on characterization of η or γ phase are available. SEM morphology of the as-sprayed WC–Co particles collected in room-temperature distilled water (Fig. 4c) showed the dense particle with spherical shape, indicating well molten state of the particles during the APS. Cross-shaped crystals with bright contrast are clearly seen (Fig. 4d). Energy spectrum analysis suggests that main chemical components of the cross-shaped crystals are Co, W and C with the Co/W/C atomic ratio of 6:6:1, a composition of η phase [24]. In addition, γ phase in nano size were also visualized in the as-sprayed WC–Co coatings (Fig. 4e and f). As clearly shown in Fig. 4e, there are some rod-like particles with a size of dozens of nanometers being embedded within the binder phase in the WC–Co coating. Closer view of the rod-like particles (Fig. 4f) together with EDS analysis suggests that those nanostructured grains adhering to WC grains are comprised of three elements, namely Co, W and C, with an atomic ratio close to that of Co(W,C) (γ phase). XRD detection shown as per Fig. 1 has already evidenced the existence of the γ phase in the WC–Co coating.

Fig. 4. FESEM images of the powders and coatings, (a, b) cross-sectional morphology of the WC–Co coatings showing island-like W and nearly complete W_2C shell around the WC particles, (c, d) FESEM images of the spherical WC–12Co particles as-sprayed in room-temperature distilled water, the closer view shows the cross-shaped η phase crystals, and (e, f) BSE images of the WC–Co coating deposited by APS at 20 kW showing rod-like shaped γ phase with a size of ~200 nm in length and ~50 nm in diameter (the white arrows point to the γ phase).

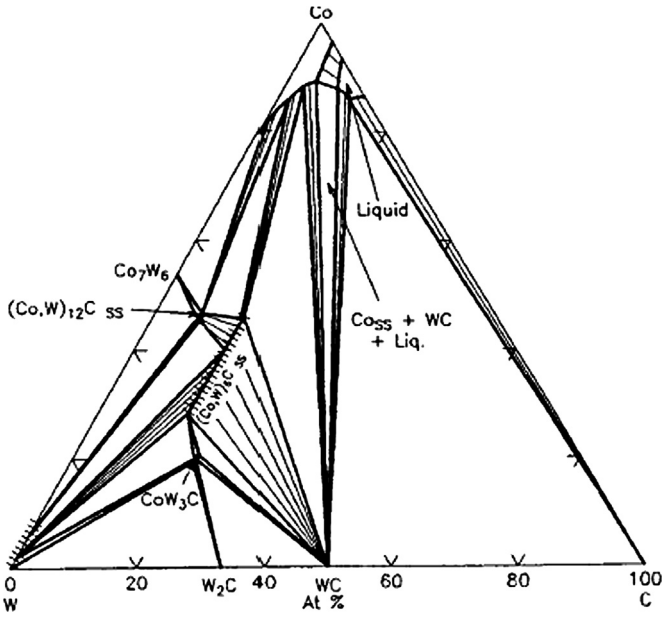

Fig. 6. The isothermal section of WC–Co phase diagram at 1425 °C, from Ref. [34].

Interestingly, the γ phase shows nano-rods shape (Fig. 4f) with the size of about 50 nm in diameter and 200 nm in length. Further research efforts are yet needed to elucidate these phenomena.

For thermal sprayed WC–Co coatings, decarburization of WC always deteriorates their mechanical properties [6,11]. The extent of the decarburization would significantly affect the performances of the coatings. The coatings showed the average microhardness value (Hv_{300}) of 1145 ± 238 at their top layers and 954 ± 178 at their bottom layers. These values are lower than that of HVOF WC–Co coatings [3], which is not surprising since severe decarburization was shown by the present APS coatings. The less decarburization at the top layer (Fig. 1) accounts for the higher microhardness value. In this work, the weight percentages of WC and C in the starting WC–Co powders and retained in the as-sprayed WC–Co and WC particles collected in distilled water were measured and calculated using the Rietveld approach from their XRD spectra, which are shown in Fig. 5. It is clear that both the WC–Co and WC particles experienced predominant decarburization during the high temperature spraying. Only 3.07wt.% WC is retained in the as-sprayed WC powders (from 100wt.% WC powders), while the percentage of WC is 14.10wt.% in the as-sprayed WC–Co powders, showing a drop of 73.90wt.% from the starting powders (14.10wt.% vs. 88.0wt.%). The content of C retained in the as-sprayed WC–Co and WC powders is 2.23% and 2.80% respectively. These nevertheless indicate the protection effect by Co on preventing decarburization of WC during the spraying. On one hand, presence of Co could alleviate the heating of WC, on the other hand, Co outer layer is capable of preventing WC from exposure to oxygen and minimizes the decarburization [32,33]. It was evidenced previously that C in the WC–Co particles diffused to their surface and got oxidized during APS. The extent of the diffusion-oxidation induced carbon loss is almost the same for both the as-sprayed WC–Co and WC particles (60.5wt.% vs. 55.2wt.% in the present study). It suggests that the advantage of Co for preventing decarburization in WC–Co particles is not associated with oxidation, but instead the diffusion-controlled carbon loss.

The formation of W_2C, W and hard phase like η, γ can be well explained by the mutual behaviors among the components during the high-temperature plasma spraying. Fig. 6 shows the phase changes in WC–Co at the temperature 1425 °C [34]. The content of Co in the powders used in the present study is 12wt.%. According to the diagram, it is reasonable that reprecipitation and decarburization of WC result in recrystallization into the phases η and γ in the present case. Based on the above microstructural features and elucidation, a model illustrating the decarburization of WC–Co

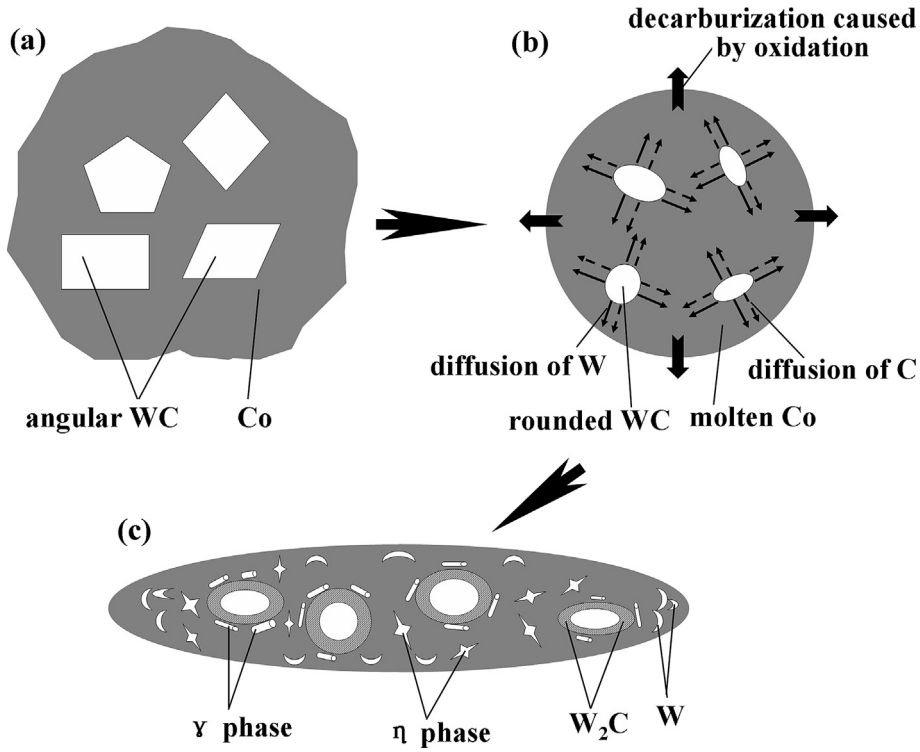

Fig. 7. Schematic depiction illustrating the decarburization behavior of WC–Co powders, (a) starting WC–Co particle showing irregular WC grains embedded in Co, (b) the particle after in-flight stage showing diffusion-controlled carbon loss, and (c) the splat after the coating formation stage showing distribution of the decarburization-induced phases.

during both in-flight and coating formation stages is schematically depicted (Fig. 7). In the original WC–Co powders, a large number of angular WC grains are bond together by binder Co (Fig. 7a). During the spraying, Co melts in the first place, followed by diffusion of W and C atoms into the liquid cobalt. As a result, the retained WC grains become smaller. At the same time, part of carbon rapidly diffuses through the liquid and gets gasified at the particle surface by, e.g., the oxidative reaction $2C + O_2 \rightarrow 2CO$ (Fig. 7b). Inhomogeneous distribution of the elements within the particle is expected, due to the different diffusion rates experienced by the atoms and the removal of carbon by oxidization. It is apparent that upon impingement of the droplet on substrate/pre-coating and subsequent flattening, the Co liquid becomes supersaturated, resulting in the formation of W_2C, W, η and γ phases, depending on the local atomic ratio (Fig. 7c). It has been well established that the decarburization extent plays important roles in determining the mechanical properties of the WC–Co coatings. The results revealed in this study shed light on further understanding the decarburization behaviors of thermal sprayed WC–Co, in turn facilitates fabrication of the coatings with super mechanical properties.

4. Conclusions

The mechanism of decarburization in plasma sprayed WC–Co coatings has been investigated. The W_2C exhibits epitaxial growth on WC grains and forms nearly complete shell around the WC particles. The η phase with its crystals being in cross shape is distributed at the surrounding part of WC–Co splats. The rod-like γ phase with a size of approximate dozens of nanometers embeds within the binder phase and is clearly well separated from WC grains. The W formed by vigorous decarburization is detected mainly in Co binder, being separated entirely away from WC grains. The controlling factor of the formation of decarburization products is un-uniform diffusion and localized precipitation. Diffusion-controlled carbon loss is presumably the predominate regime for the formation of W_2C in the coatings.

Acknowledgment

The authors thank Dr. Jinling Xu from Rensselaer Polytechnic Institute for her help on Rietveld refinement of the data. This research was supported by 100 Talents Program of Chinese Academy of Sciences (to H.L.).

References

[1] J.M. Guilemany, J.M. Depaco, J. Nutting, J.R. Miguel, Metall. Mater. Trans. A 30 (8) (1999) 1913.
[2] C. Verdon, A. Karimi, J.L. Martin, Mater. Sci. Eng. A 246 (1–2) (1998) 11.
[3] D.A. Stewart, P.H. Shipway, D.G. McCartney, Wear 225–229 (1999) 789.
[4] R. Schwetzke, H. Kreye, J. Therm, Spray Technol. 8 (1999) 433.
[5] H. Chen, I.M. Hutchings, Surf. Coat. Technol. 107 (1998) 106.
[6] P. Suresh Babu, B. Basu, G. Sundararajan, Wear 268 (2010) 1387.
[7] P. Suresh Babu, B. Basu, G. Sundararajan, Acta Mater. 56 (2008) 5012.
[8] H. Du, W. Hua, J. Lu, J. Gang, C. Sun, L. Wen, Mater. Sci. Eng. A 408 (2005) 202.
[9] D.G. Giovanni, P. Luciano, P. Giovanni, M. Francesco, J. Am. Ceram. Soc. 92 (2009) 1118.
[10] Y. Qiao, T.E. Fischer, A. Dent, Surf. Coat. Technol. 172 (2003) 24.
[11] S.Y. Park, M.C. Kim, C.G. Park, Mater. Sci. Eng. A 449–451 (2007) 894.
[12] J.M. Guilemany, S. Dosta, J. Nin, J.R. Miguel, J. Therm. Spray Technol. 14 (2005) 405.
[13] D.A. Stewart, P.H. Shipway, D.G. McCartney, Acta Mater. 48 (2000) 1593.
[14] P. Suresh Babu, D.S. Rao, G.V.N. Rao, G. Sundararajan, J. Therm. Spray Technol. 16 (2) (2007) 281.
[15] B.H. Kear, G. Skandan, R.K. Sadangi, Scripta Mater. 44 (2001) 1703.
[16] R. Bao, J.H. Yi, Y.D. Peng, H.Z. Zhang, A.K. Li, Trans. Nonferrous Met. Soc. China 22 (2012) 853.
[17] Q. Zhan, L.G. Yu, F.X. Ye, Q.J. Xue, H. Li, Surf. Coat. Technol. 206 (2012) 4068.
[18] H.M. Rietveld, J. Appl. Crystallogr. 2 (1969) 65.
[19] D. Mari, L.M. Berger, S. Stahr, Solid State Phenom. 184 (2012) 313.
[20] K. Yang, Y. Ebisuno, K. Tanaka, M. Fukumoto, T. Yasui, M. Yamada, Surf. Coat. Technol. 205 (2011) 3816.
[21] S. Chandra, P. Fauchais, J. Therm. Spray Technol. 18 (2) (2009) 148.
[22] V.V. Sobolev, J.M. Guilemany, J.A. Calero, J. Mater. Process. Technol. 96 (1999) 1.
[23] A. Ohmori, C.J. Li, Thin Solid Films 201 (1991) 241.
[24] C.J. Li, A. Ohmori, Y. Harada, J. Therm. Spray Technol. 5 (1996) 69.
[25] M.S.A. Khan, Ph.D. thesis, University of Cambridge, 1998.
[26] I. Konyashin, B. Ries, F. Lachmann, A.T. Fry, J. Mater. Sci. 47 (2012) 7072.
[27] C.J. Li, A. Ohmori, Y. Harada, J. Mater. Sci. 31 (1996) 785.
[28] http://srdata.nist.gov/xps.
[29] V.I. Nefedov, M.N. Firsov, I.S. Shaplygin, J. Electron Spectrosc. Relat. Phenom. 26 (1982) 65.
[30] I. Kojima, M. Kurahashi, J. Electron Spectrosc. Relat. Phenom. 42 (1987) 177.
[31] R. Nieminen, P. Vuoristo, K. Niemi, T. Mäntylä, G. Barbezat, Wear 212 (1997) 66.
[32] J.H. Yuan, Y.C. Zhu, X.B. Zheng, H. Ji, T. Yang, J. Alloys Compd. 509 (2011) 2576.
[33] A.K. Basak, S. Achanta1, M.D. Bonte, J.P. Celis, M. Vardavoulias, P. Matteazzi, T. I. Met. Finish 85 (2007) 310.
[34] A.E. McHale, Phase Equilibria Diagrams – Phase Diagrams for Ceramists, vol. 10, The American Ceramic Society, Westerville, Ohio, 1994.